J. Mod. Power Syst. Clean Energy (2019) 7(5):1340–1354
https://doi.org/10.1007/s40565-019-0560-3

Soft-switching SiC power electronic conversion for distributed energy resources and storage applications

Keyan SHI[1], Jinyi DENG[1], An ZHAO[1], Dehong XU[1]

Abstract Power electronic conversion plays an important role in flexible AC or DC transmission and distribution systems, integration of renewable energy resources, and energy storage systems to enhance efficiency, controllability, stability, and reliability of the grid. The efficiency and reliability of power electronic conversion are critical to power system applications. One way to enhance the efficiency and reliability of power electronic conversion is soft-switching technology. This paper introduces a generic zero-voltage-switching (ZVS) technique based on silicon carbide (SiC) power device. Using the proposed ZVS technique, all semiconductor switching devices in a power converter can realize ZVS operations. Next, the applications of the ZVS technique in different power electronic conversion systems such as photovoltaic inverters, wind power systems, energy storage systems and flexible AC transmission system devices are discussed. Finally, as an example, the operation performance and efficiency improvement of a SiC metal-oxide-semiconductor field-effect transistor (MOSFET) ZVS back-to-back converter are discussed.

Keywords Power electronic conversion, Flexible AC transmission systems (FACTS), Soft-switching, SiC MOSFET, Distributed energy resources

CrossCheck date: 28 April 2019

Received: 21 November 2018 / Accepted: 28 April 2019 / Published online: 20 August 2019

✉ Dehong XU
xdh@cee.zju.edu.cn

Keyan SHI
skyshi@zju.edu.cn

Jinyi DENG
dengjinyi@zju.edu.cn

An ZHAO
zhaoan@zju.edu.cn

[1] College of Electrical Engineering, Zhejiang University, Hangzhou 310027, China

1 Introduction

The increasing applications of renewable energy and distributed power generation have become a driving force for an increasing use of power electronic conversion in power systems [1]. Power electronic conversion is now playing an ever important role in the grid. More efficient and more reliable power converters/inverters are required. At present, silicon-based power semiconductor devices such as silicon controlled rectifier (SCR) and insulated gate bipolar transistor (IGBT) are widely used. With regard to IGBT, its switching frequency is limited owing to its switching loss. The limitation of switching frequency further restricts the dynamic characteristics of the flexible AC transmission system (FACTS) device. Besides, this also causes larger passive components such as inductors, capacitors, and transformers.

To meet the ever-increasing demands for higher performance of power electronic conversion, a revolutionary development in the power switching device technology has taken place. This development exploits wide bandgap (WBG) materials such as silicon carbide (SiC) and gallium nitride (GaN). The WBG power device has intrinsic material physical advantages over the traditional silicon device. These advantages enable a higher blocking voltage, higher switching frequency, and higher operating temperature [2, 3]. Its low loss and high blocking voltage make it

possible to utilize simpler power conversion topologies such as two-level converters. The application of SiC-based power conversion in utilities, including the FACTS devices, power electronic interfaces for distributed energy resources, and energy storage systems, can significantly improve the efficiency and reliability of the system, and reduce the system weight and volume. Therefore, it is a promising technology for future flexible power systems with high-penetration renewable energy.

However, the electro-magnetic interference (EMI) noise and switching loss continue to be concerns in respect of the SiC device, as is the case with their silicon counterparts. The intrinsic fast switching characteristics of the SiC device result in more severe EMI noise than that in the silicon device [4]. When the switching frequency increases beyond tens of kHz, the switching loss is still a bottleneck for the enhancement of the efficiency and power density. To further enhance the performance of SiC-device-based power converters, soft-switching technique is a promising technology, and can handle the aforementioned concerns by turning the power device on and off with a slower voltage and current slope to reduce EMI noise. Furthermore, the switching loss is remarkably reduced by displacing the overlapping area of the voltage and current waveforms during the switching transient process. Therefore, higher efficiency and less EMI noise can be achieved for SiC power conversion systems with an increasing switching frequency. The increase in the switching frequency brings extra benefits. One benefit is the miniaturization of power converter, which is beneficial for applications where space is a constraint owing to volume reductions in passive components. The second benefit is that a higher switching frequency results in a wider control bandwidth and faster dynamics of the system. It would be helpful in fault ride through and system stability control.

Power electronic conversion systems applied in the power systems are basically single-phase or three-phase DC/AC converters. Based on the location of the auxiliary circuit, the DC/AC soft-switching technique can be generally classified into two categories: DC-side soft-switching technique and AC-side soft-switching technique. The DC-side soft-switching technique usually has one simple auxiliary circuit installed in the DC-side. A well-known inverter with the DC-side soft-switching technique is the DC resonate link inverter or active clamping DC resonate link inverter [5–8]. It can realize soft-switching for all switches. However, it has a lower efficiency owing to the higher voltage and current stress on the switches and variable switching frequency control. In the AC-side soft-switching technique, the auxiliary circuits are placed at each AC output node of the phase leg. It has complex auxiliary circuits, especially when there are multiple phase legs in the circuit topology [9–11].

To overcome the drawbacks of the DC resonate link inverter, a novel fixed-switching-frequency zero-voltage-switching pulse width modulation (ZVS-PWM) technique for the DC-side resonation method has been investigated in [12–15]. In the proposed zero-voltage-switching (ZVS) technique, only one simple auxiliary circuit is employed to realize the ZVS operation for all power switching devices. It has been successfully applied to the three-phase inverter and rectifier, single-phase inverter and so on. ZVS-SVM and zero-voltage-switching sinusoidal pulse width modulation (ZVS-SPWM) schemes are proposed to realize the ZVS operation of all switching devices for both three-phase three-wire and three-phase four-wire systems. Actually, these ZVS circuit topologies have a similar operation principle and modulation scheme, and their analytical methods can be unified and further expanded to other circuit topologies.

In this paper, a generic ZVS technique concept is firstly introduced based on the multi-phase ZVS converter [16]. The basic operating principle and ZVS-PWM scheme are presented. These are applicable for different ZVS circuit topologies derived from the generic ZVS technique concept. Next, the applications of the ZVS technique in renewable energy integration, energy storage system and FACTS devices are investigated. Their system improvements of performance in regard to efficiency, dynamic response, and footprint of passive components are discussed according to different application scenarios. Because wide-bandgap devices such as SiC metal-oxide-semiconductor field-effect transistor (MOSFET) have less turn-off loss than turn-on loss, ZVS operation will bring more significant efficiency improvements in these power electronic conversion systems. Finally, experiment results on a 10 kVA ZVS back-to-back (BTB) converter prototype using a SiC MOSFET validate the efficiency improvement compared with that of the conventional two-level hard-switching BTB converter.

2 Concept of generic ZVS technique

In this section, a generic ZVS technique is introduced, which includes a generic *N*-bridge ZVS circuit topology and its ZVS-PWM scheme [16]. A group of ZVS converters can be derived from the generic *N*-bridge ZVS circuit topology.

2.1 Generic *N*-bridge ZVS circuit topology

In general, there are three types of switching losses, namely, turn-on, turn-off, and reverse recovery losses, in the conventional hard-switching converter. We take a half bridge, shown in Fig. 1, as an example. It is assumed that

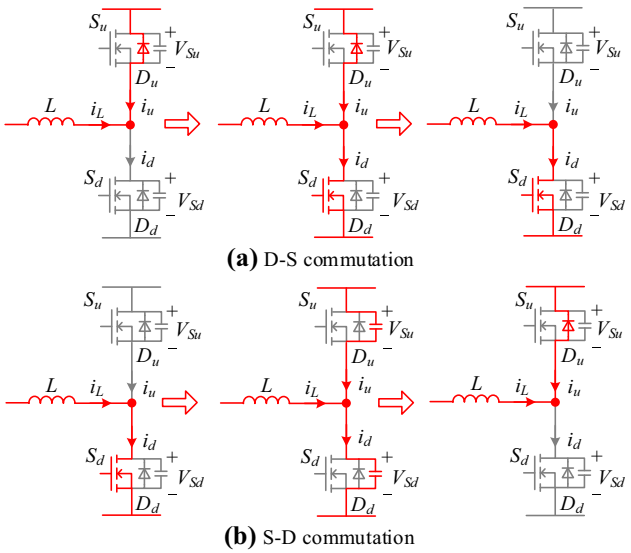

Fig. 1 Current commutations for hard-switching converter

current i_L injected into the midpoint of the bridge leg is positive. Typically, there will be two different current commutation processes in one switching period. The first one is from the diode to its complementary switch as shown in Fig. 1a, which is termed as the D-S commutation process. In the D-S commutation, the diode will undergo a serious reverse recovery process, which will cause a reverse recovery loss and increase the turn-on loss for its complementary switch. The other commutation type is from the main switch to the diode of its complementary switch as shown in Fig. 1b, which is termed as the S-D commutation process. In the S-D commutation process, the diode is freewheeling when its complementary switch is turned off. The turn-off loss may be reduced if there is a capacitor in parallel with the switch.

Figure 2a shows the typical voltage and current waveforms as well as the power loss distribution of these two commutation processes, where V_{Su}, i_u, V_{Sd}, i_d are voltage and current of the switches S_u and S_d. The shaded areas denote the switching processes. E_{on}, E_{off}, and E_{rr} represent

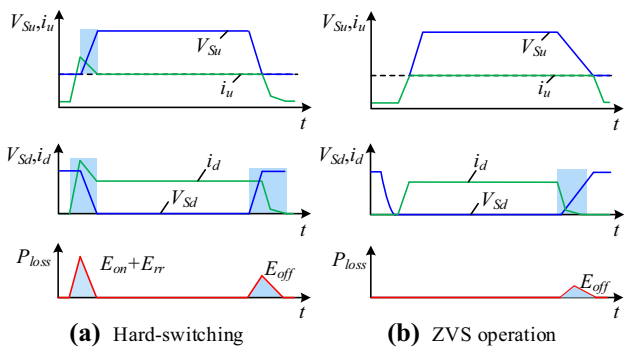

Fig. 2 Switching waveform and power loss

energy losses during the turn-on, turn-off, and reverse recovery process, respectively.

The basic idea of the proposed ZVS technique is to use an auxiliary circuit to resonate the voltage across the switches to zero before the instant of each D-S commutation. Figure 3 shows the circuit diagram of the ZVS technique with one phase leg. The auxiliary circuit includes resonant inductor L_r, auxiliary switch S_a and clamping capacitor C_c. Besides, external resonant capacitors C_u, C_d, and C_a are in parallel with each switch as the resonant capacitors.

For most of the time in a switching period, auxiliary switch S_a is in the "on" state, and a current circulates in the auxiliary circuit. Once auxiliary switch S_a is turned off, energy in resonant inductor L_r will resonate DC bus voltage V_{bus} to zero. Then the main switches can be turned on with ZVS condition. In this way, the traditional D-S commutation process is avoided. Figure 2b shows the voltage and current waveforms as well as the power loss distribution with the ZVS operation. The turn-on and reverse recovery loss can be totally eliminated, while the turn-off loss is also cut down owing to the existence of resonant capacitors in parallel to each switch.

When more bridge legs are connected to the DC bus, the ZVS concept can be further extended to an N-bridge circuit topology [16], as shown in Fig. 4. In each half bridge, there will be a D-S commutation process in every switching period according to the direction of its inductor current. Before these D-S commutation instants, the auxiliary circuit will act and resonate DC bus voltage V_{bus} to zero. In this way, all the main switches can realize ZVS operation.

2.2 ZVS-PWM scheme

In the traditional pulse width modulation scheme, a triangular carrier is usually adopted to generate symmetric PWM waveforms. The duty cycles for each arm are obtained by comparing the corresponding modulation signals (m_1, m_2, …, m_N) with the triangular carrier. The upper and lower switching devices in each arm are switched in a complementary manner. Figure 5a shows the typical

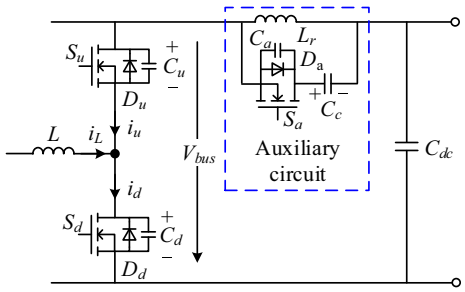

Fig. 3 ZVS circuit topology with one phase leg

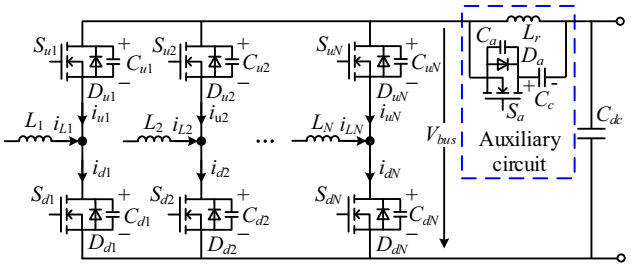

Fig. 4 Generic *N*-bridge ZVS circuit topology

driving signal waveforms (u_{g_u1}, u_{g_d1}, u_{g_u2}, u_{g_d2}, …, u_{g_uN}, u_{g_dN}) for the *N*-bridge converter. The D-S commutation instants as shown with vertical red-line marks for *N* different bridge legs, are distributed in different moments of a switching period. Therefore, for the traditional SPWM scheme, the auxiliary circuit might need to act *N* times in one switching period to provide the ZVS condition for each bridge, which will cause extra loss for the auxiliary switch.

To reduce the action times of the auxiliary circuit, the D-S commutation instants are rearranged by changing the triangular carrier to a saw-tooth carrier as shown in Fig. 5b. In this way, the D-S commutation instants for all the *N* bridges are aligned. Therefore, the auxiliary circuit only needs to operate once during each switching period, and ZVS turn-on of the *N* main switches can be achieved simultaneously. u_{ga} denotes the driving signal of the auxiliary switch. It should be noted that the equivalent area principle of PWM modulation in each switching period still holds in the proposed ZVS-PWM method.

2.3 Operation principle of ZVS technique

The basic operating principle of the ZVS technique is illustrated using the one-phase-leg ZVS converter in Fig. 3, which can be easily expanded to the *N*-bridge ZVS converter. Figure 6 shows the operation stages of the one-phase-leg ZVS converter. Figure 7 shows the corresponding key waveforms in one switching period, where V_{gu}, V_{gd}, and V_{ga} represent the gate-driving signals for S_u, S_d, and S_a, respectively. Stages 1 through 6 are introduced in detail to present the D-S commutation process and ZVS operation of the switching devices.

In stage 1 (t_0–t_1), D_u is conducting and S_a is in the "on" state. The resonant inductor current is increasing at the rate of $\mathrm{d}i_{Lr}/\mathrm{d}t = V_{Cc}/L_r$.

In stage 2 (t_1–t_2), the first resonation will resonate V_{bus} to zero by turning off S_a, which provides the ZVS condition for S_d. At the same time, u_{Ca} is resonated to $V_{dc} + V_{Cc}$. This stage ends when V_{bus} is resonated to zero.

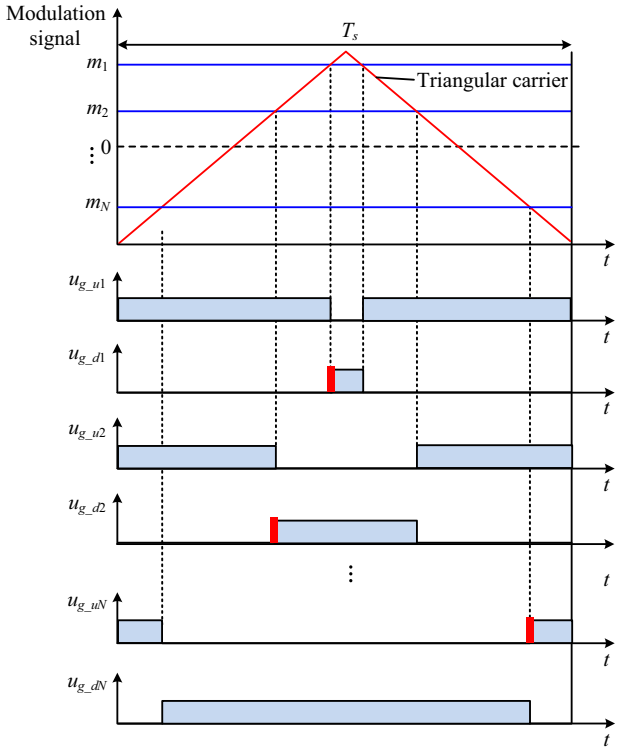

(a) Traditional SPWM scheme

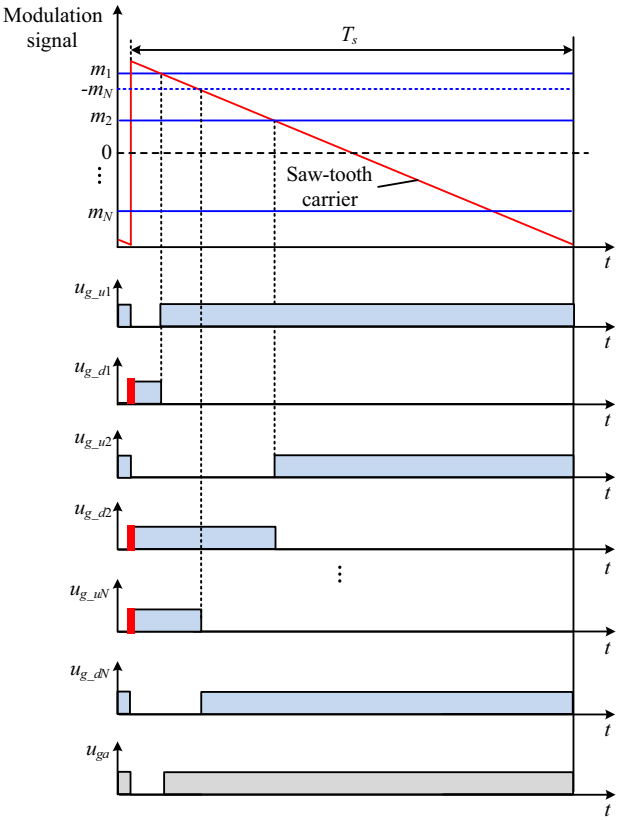

(b) ZVS-PWM scheme

D-S commutation instants

Fig. 5 Traditional SPWM scheme and ZVS-PWM scheme

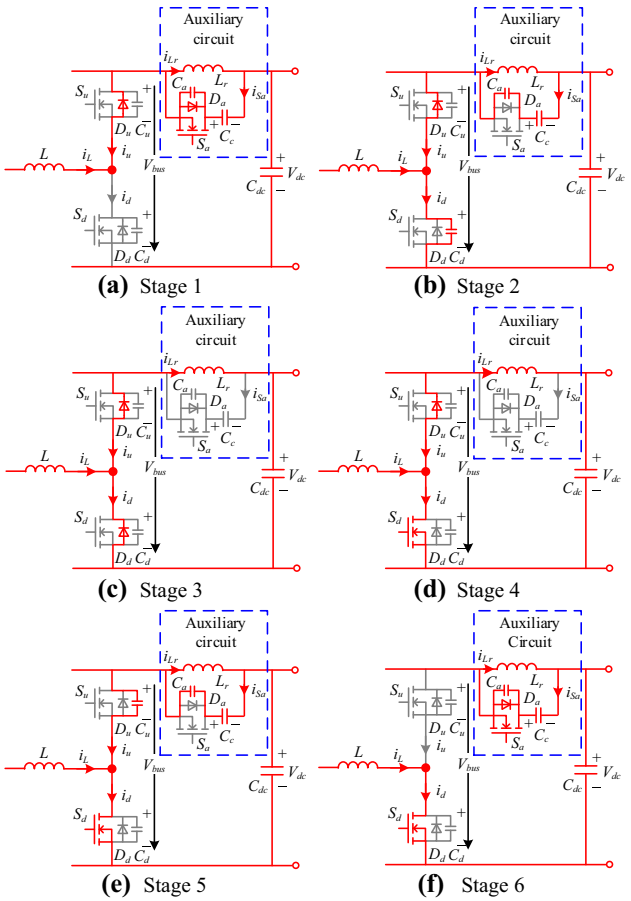

Fig. 6 Operation stages

In stage 3 (t_2–t_3), S_d is the ZVS turned on. The voltage across the resonant inductor is clamped to V_{dc}, and its current decreases with a slope of $di_{Lr}/dt = -V_{dc}/L_r$.

In stage 4 (t_3–t_4), the current in diode D_u will be commutated to S_d. Unlike the hard-switching converter case, the D-S commutation process here is suppressed owing to the existence of L_r. When i_u decreases to zero, this stage ends.

In stage 5 (t_4–t_5), the second resonation will happen immediately after the D-S commutation. The voltage across S_a will be resonated to zero, whereas the voltage across S_u will be resonated to $V_{Cc} + V_{dc}$. After u_{Ca} resonates to zero, S_a will be turned on with ZVS condition.

In stage 6 (t_5–t_6), S_d is conducting and the voltage across the resonant inductor will be continuously clamped to V_{Cc}. Actually, the converter will operate just as the conventional PWM converter after stage 6. So stages after this are not given in detail.

When the circuit works in steady state, the resonant inductor should meet the voltage-second balance principle in one switching period. Neglecting the short resonation stages, the following equation should be met:

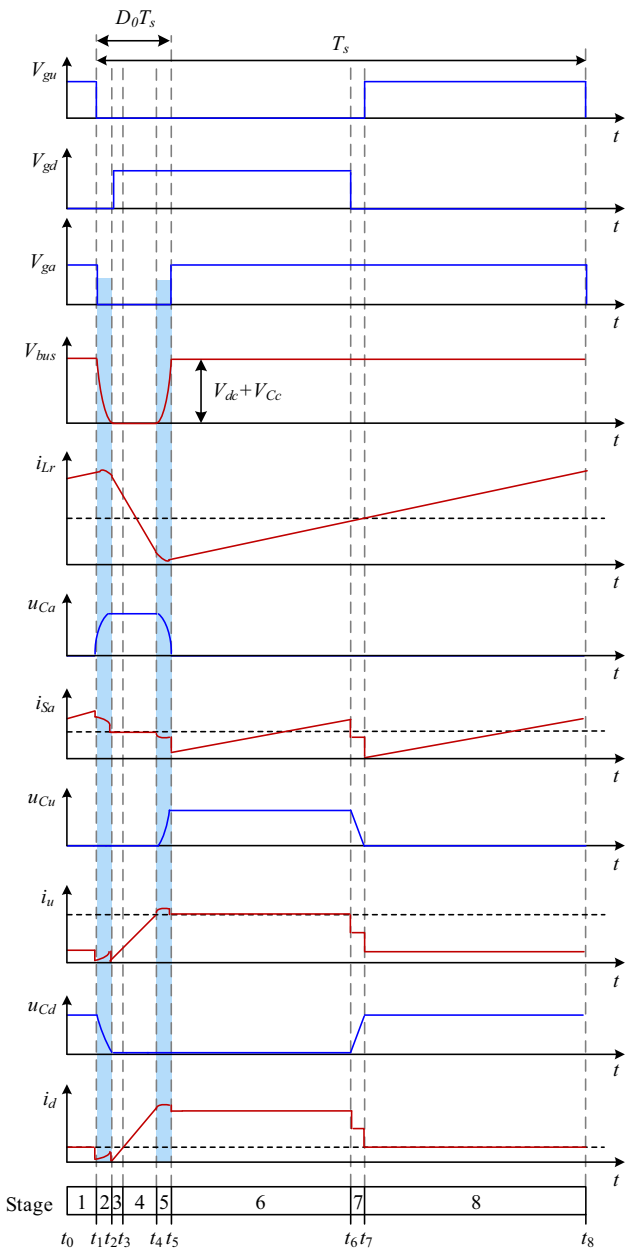

Fig. 7 Key waveforms in one switching period

$$\int_0^{T_s} V_{Lr}(t)\mathrm{d}t = V_{Cc}(1-D_0)T_s - V_{dc}D_0T_s = 0 \tag{1}$$

where T_s is the switching period; V_{Lr} is the voltage across the resonant inductor; and D_0 is the turn-off duty cycle of the auxiliary switch, as shown in Fig. 7. Then the relationship between clamping capacitor voltage V_{Cc} and D_0 can be written as:

$$V_{Cc} = D_0V_{dc}/(1-D_0) \tag{2}$$

Clamping capacitor C_c should also obey the ampere-second balance principle in one switching period.

Neglecting the resonation and short S-D commutation stages, the following equation can be obtained:

$$\int_0^{T_s} i_{Sa}(t)\mathrm{d}t = \int_{t_3}^{t_4} i_{Sa}(t)\mathrm{d}t + \int_{t_5}^{t_6} i_{Sa}(t)\mathrm{d}t + \int_{t_7}^{t_8} i_{Sa}(t)\mathrm{d}t = 0 \tag{3}$$

The duration of each stage in (3) is decided by the duty cycle of each phase, which is related to its modulation index M. Then the expression for the turn-off duty cycle of the auxiliary switch for the one-bridge-leg ZVS converter can be derived as:

$$D_0 = \frac{L_r\left[\frac{2V_{dc}}{Z_r} + (M+1)|i_L|\right]}{V_{dc}T_s} \tag{4}$$

When expanding to the N-bridge ZVS topology circuit, a generic expression for the turn-off duty cycle of the auxiliary switch can be written as:

$$D_0 = \frac{2L_r\left(\frac{V_{dc}}{Z_r} + |i_{dc}| + \frac{1}{2}\sum_{n=1}^{N}|i_{Ln}|\right)}{V_{dc}T_s} \tag{5}$$

where i_{Ln} is the phase current for phase n; Z_r is the resonation impedance; and i_{dc} is the average DC link current. They can be expressed as:

$$\begin{cases} Z_r = \sqrt{L_r/[(N+1)C_r]} \\ i_{dc} = \dfrac{1}{2}\displaystyle\sum_{n=1}^{N} i_{Ln}M_n \end{cases} \tag{6}$$

where M_n is the modulation index for each phase leg and C_r is the resonant capacitor paralleled to each switch. By designing the turn-off duty cycle of the auxiliary switch as in (5), both the voltage-second balance principle and ampere-second balance principle for the resonant inductor and clamping capacitor can be fulfilled, and the auxiliary circuit will operate in the steady state.

3 Application of ZVS converter

The proposed ZVS technique can be applied in different circuit topologies in which the half bridge is used as the basic circuit unit, such as the traditional two-level AC/DC or DC/AC converters and bidirectional buck-boost DC/DC converters. Besides, double-stage or multi-stage converters with a common DC bus can also adopt the ZVS technique. This section introduces the applications of these ZVS topologies in power electronic conversion systems for renewable energy integration, energy storage systems and FACTS devices.

3.1 Integration of renewable energy

Figure 8 shows the topology of the single-phase ZVS DC/AC inverter for a low-power photovoltaic (PV) system. The traditional H-bridge single-phase inverter has very simple circuit structure [17]. However, the silicon MOSFET device used in the topology limits its switching frequency owing to the poor reverse recovery performance of its body diode. By introducing the ZVS technique, the diode reverse recovery process is avoided, and its switching frequency can increase from many tens of kHz to over 100 kHz, which can significantly reduce the volume and weight of the entire system.

In the single-phase PV inverter, power flowing into the grid fluctuates with double-line frequency. This double-line frequency power pulsation appears in the DC-side if no power decoupling measures are taken. A typical power decoupling method is to use a buck-type stage to actively absorb power pulsation [18]. Using this technique can help avoid the large DC electrolytic capacitors. However, the active power decoupling (APD) stage will cause extra switching loss and impact the system efficiency. Both the APD and single-phase DC/AC stages can realize ZVS operation by introducing the ZVS technique and the system efficiency and power density can be improved, as shown in Fig. 9.

Similarly, a boost DC/DC stage will be cascaded with the inverter for a wider input voltage range, as shown in Fig. 10 in certain PV applications. This additional conversion stage will also cause extra loss. By using one auxiliary circuit, both the boost stage and the single-phase DC/AC stage can realize soft-switching operation. The increase in the switching frequency can make the system more compact.

The three-phase three-wire DC/AC inverter is widely used in the centralized PV power generation system. The most commonly used central inverter topology is the two-level voltage source inverter (2L-VSI). The 2L-VSI has a very simple structure; it is composed of three half-bridge phase legs connected to a single DC link. However, the traditional 2L-VSI suffers from high switching losses

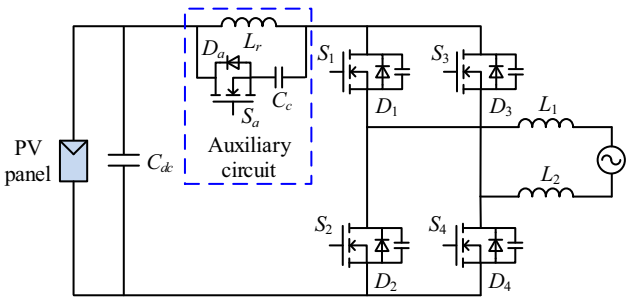

Fig. 8 Single phase ZVS DC/AC inverter for PV system

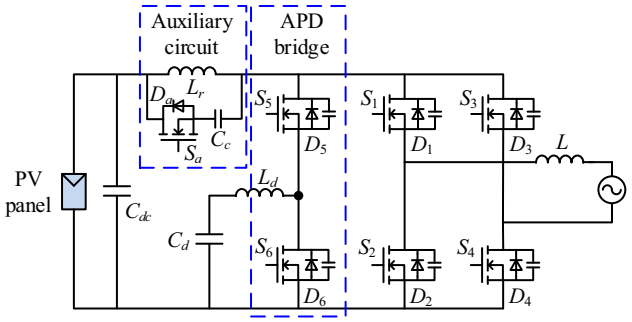

Fig. 9 Single-phase ZVS inverter with APD module for PV system

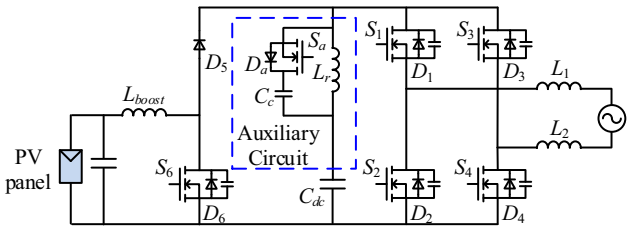

Fig. 10 Double-stage single-phase ZVS inverter for PV system

owing to its hard-switching operation, which actually limits the operation switching frequency and leads to a bulky filter. In practical high–power centralized PV systems, the 2L-VSI with the IGBT device usually operates at 10 kHz switching frequency. If a high-power SiC MOSFET module is applied, the switching frequency can increase by three to five times that of the IGBT module. To further increase the switching frequency of the inverter, the ZVS technique can be used in the SiC MOSFET PV inverter, as shown in Fig. 11. The ZVS inverter prototype in [19] shows a high efficiency of 98.6% at a 300 kHz switching frequency compared to that of the hard-switching topology operating at a 100 kHz switching frequency with a similar conversion efficiency.

Another important circuit topology used in distributed and centralized PV generation systems is the string inverter [20]. The string inverter is basically composed of two conversion stages: the DC–DC and DC–AC stages. The DC–DC stage is adopted to extend the PV voltage operation region and harvest more energy. Usually multiple DC–DC boost converters, as shown in Fig. 12, are connected in

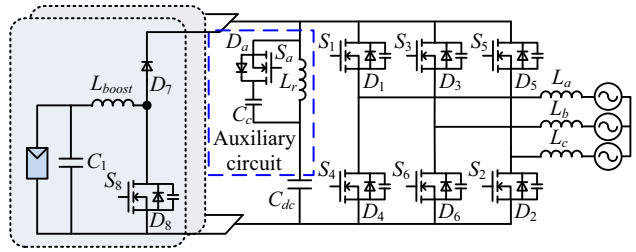

Fig. 12 Double-stage three-phase ZVS inverter for PV system

parallel to increase the maximum power point tracking (MPPT) efficiency and power capacity as well. However, the two-stage configuration will have more components and cause extra power loss during energy conversion. By introducing the ZVS technique, higher switching frequency can be achieved and the power density can be enhanced.

Besides PV inverters, the ZVS technique can also be applied in the power electronic conversion of the wind power system. Two most popular wind power conversion systems are based on the doubly fed induction generator (DFIG) and permanent magnet synchronous generator (PMSG) [21]. Both utilize a BTB converter to interface the generator side and the grid side. The BTB converter for the PMSG system with the ZVS technique is shown in Fig. 13. In a typical wind power system, the entire power converter is packed in a cabinet and placed in a nacelle with limited space. The ZVS BTB converter may operate with higher switching frequency, hence the volume and weight of the passive components can be significantly reduced. The reduced size and weight of the power converter can spare more room in the nacelle. In this way, a step-up transformer can be accommodated in the nacelle to reduce the cable cost and energy losses.

To further enhance the power capacity of the wind power generation system, higher voltage levels are preferred to realize a cost-effective system design. The three-level *H*-bridge BTB converter is composed of two three-phase *H*-bridge converters. It can generate more voltage levels and handle higher power capacities, which is suitable for the high-voltage and high-power wind power generation system. The ZVS three-level *H*-bridge BTB converter is shown in Fig. 14. By introducing one auxiliary

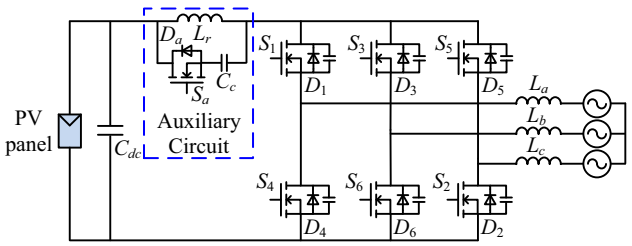

Fig. 11 Three-phase ZVS inverter for PV system

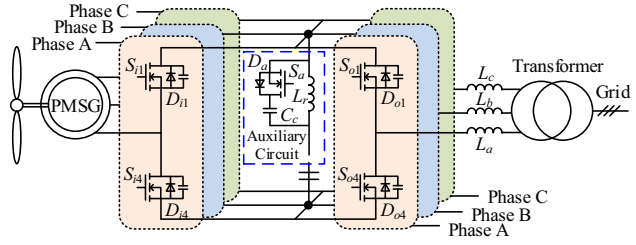

Fig. 13 ZVS back-to-back converter for PMSG system

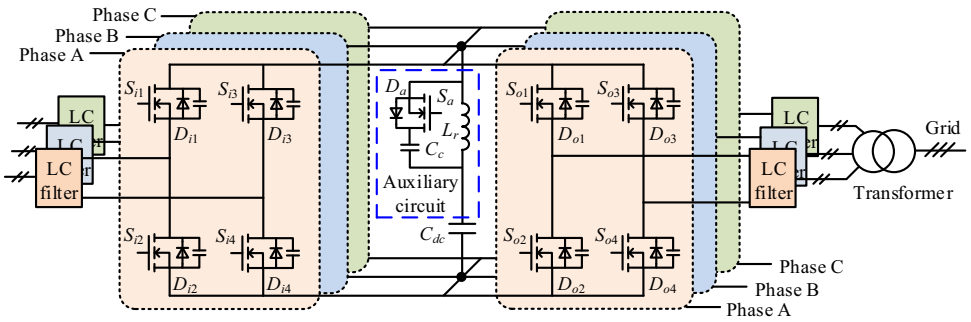

Fig. 14 ZVS three-level *H*-bridge back-to-back converter

circuit, ZVS operation for all the bridge legs can be realized. Similar benefits of volume and weight reduction can be expected.

3.2 Energy storage system

Energy storage systems have become a key enabling technology for a robust, highly efficient and cost-effective power grid. Grid level energy storage systems are used in frequency regulation, spinning reverse, peak shaving, load leveling, and so on. Besides, energy storage systems are also introduced in distributed systems to stabilize the power output of renewable energy [22, 23]. The power electronic conversion system is the interface to connect the energy storage system with the power grid. Typical energy storage systems require a bidirectional power flow control for the power electronic conversion system such as the battery energy storage system (BESS). The energy loss is also doubled during the whole energy utilization cycle by charging and discharging the energy storage device. In this regard, the improvement of efficiency of the power conversion system will be more significant as compared with that of the unidirectional power flow system. The ZVS technique can effectively improve the efficiency of the power electronic conversion system, which will make it a potential technology in the energy storage application.

The power conversion system (PCS) for the BESS can be divided into single-stage and double-stage structures. For the single-stage PCS, the battery voltage should not fluctuate widely during the discharging or charging process, which is typically related to the characteristics of the battery technology. Usually the energy-type battery is more suitable for this type of converter interface, because its output voltage is more stable during different states of charge (SOC). Therefore, this type of BESS is more suitable for large-scale energy management applications [24]. Moreover, the efficiency of the power converter will be more significant for this kind of system. The single-stage three-phase voltage source converter (VSC) is a typical PCS topology for the battery energy storage application. Similarly, the ZVS technique can be implemented as its application in the PV system, as shown in Fig. 11. To extend the system power capacity and improve fault tolerance, a PCS structure with parallel three-phase two-level VSCs might be adopted, as shown in Fig. 15. The ZVS technique can be applied in the topology by installing the auxiliary circuit in the common DC bus. Both VSCs can realize the ZVS operation while only one auxiliary circuit is adopted.

The double-stage PCS consists of a bidirectional DC/DC conversion stage and a DC/AC stage. The DC/DC stage boosts the battery voltage to the suitable level so that the inverter stage can be directly interfaced to the grid. This type of PCS is suitable for the maximum utilization of the battery stored energy. In these applications, the battery usually has a low Ampere-hour capacity, but it can discharge with a large current rate. Its output voltage will have a wider variation during the entire SOC. Figure 16 shows the bidirectional double-stage PCS with the ZVS technique.

The double-stage interface has the advantage of a common DC bus line. Different energy storage units can be integrated to the system, which makes the system more expandable and fault tolerant [25]. Figure 17 shows the diagram of the double-stage interface with parallel DC/DC

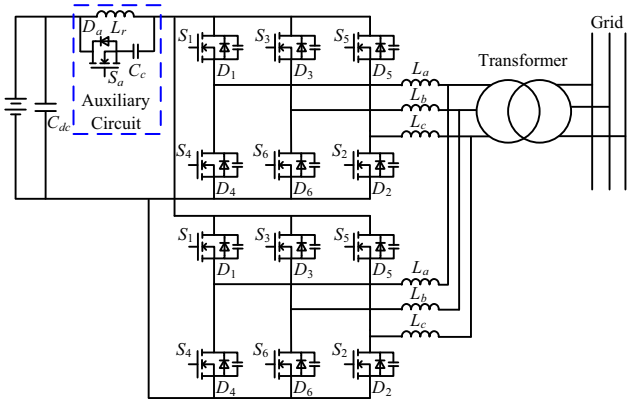

Fig. 15 Paralleled three-phase ZVS inverter for ESS

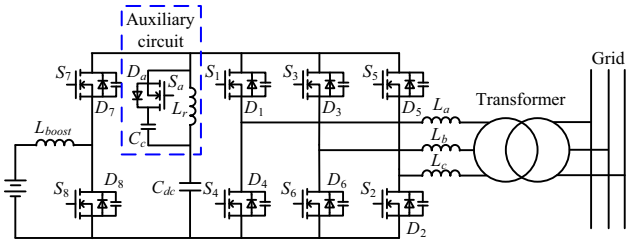

Fig. 16 Bidirectional double-stage ZVS inverter for BESS

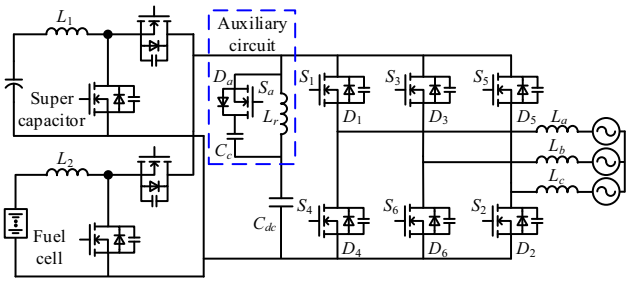

Fig. 17 ZVS inverter with paralleled DC/DC converters for BESS

converter modules integrating the fuel cell stack and supercapacitor stack. All the converters connected to the DC bus can realize ZVS operation with only one auxiliary circuit in the middle DC link. Further extension to multiple energy sources system can be obtained, as shown in Fig. 18. Different types of energy storage device (ESD) can be integrated by either the DC/DC or AC/DC converter to the DC bus line with one auxiliary circuit. More efficiency benefits are obtained because all the converters connected to the DC bus can realize the soft-switching operation with only one auxiliary circuit.

3.3 FACTS device

Power electronic conversion plays an important role in improving the reliability, power quality and efficiency of power grid. Some of these require voltage-blocking capabilities of the order of tens and hundreds of kV. Traditional SiC devices are connected in series to achieve a high blocking voltage. The future SiC device with higher blocking voltages of up to tens of kV will meet the voltage requirement with one single device or with fewer devices connected in series. Therefore, simple structures such as two-level converters can be utilized in such applications. The soft-switching technique can also be introduced to deal with the EMI problem and enable higher switching frequency.

Reactive power compensation is a major objective for FACTS devices [26]. It can be implemented with var generators connected in parallel or in series. Shunt reactive power compensation devices such as static var compensators (STATCOMs) can provide a continuous and precise leading or lagging reactive power to improve the voltage stability of the power system. By introducing the ZVS technique along with the SiC device, the whole system can be more compact and more efficient. Owing to their small sizes, these STATCOMs are more suitable for applications where space is a consideration.

A shunt active power filter (APF) is usually installed near the nonlinear load for the compensation of the harmonic current generated by the nonlinear load [27]. The power converter can operate with higher switching frequency with the ZVS technique. The advantage resulting from higher switching frequency is that a wider control bandwidth for the harmonic current control loop can be achieved, which will have better harmonic mitigation performance owing to more precise control of each harmonic current [28]. Figure 19 shows the ZVS two-level converter for the APF application with the SiC device. The same topology can also be utilized in STATCOM or static var generator (SVG) [29].

The series var compensation can increase the angular and voltage stability of the power corridor. Typical series var compensators are: static synchronous series compensator (SSSC) [30] and dynamic voltage restorer (DVR) [31]. These FACTS devices can also benefit from the application of the ZVS technique in regard to the reduced system volume and fast control response. Figure 20 shows the typical DVR topology using the ZVS technique.

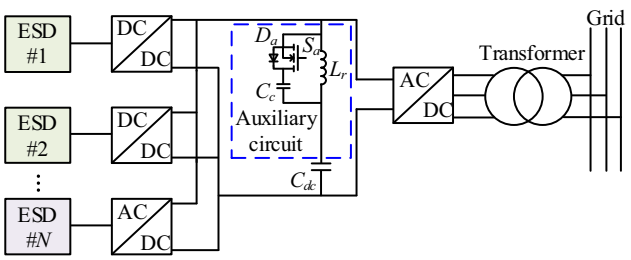

Fig. 18 Multiple energy storage system with ZVS converters

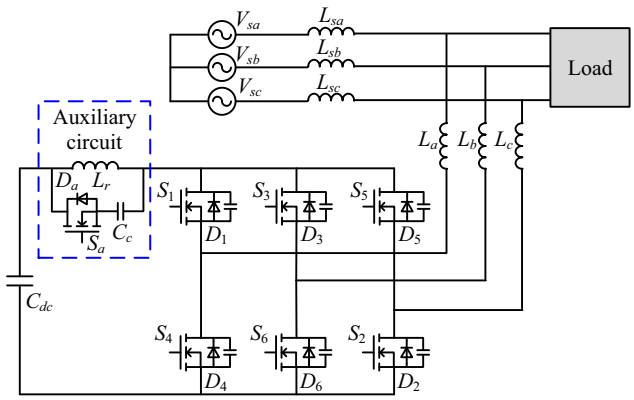

Fig. 19 ZVS inverter for APF/STATCOM

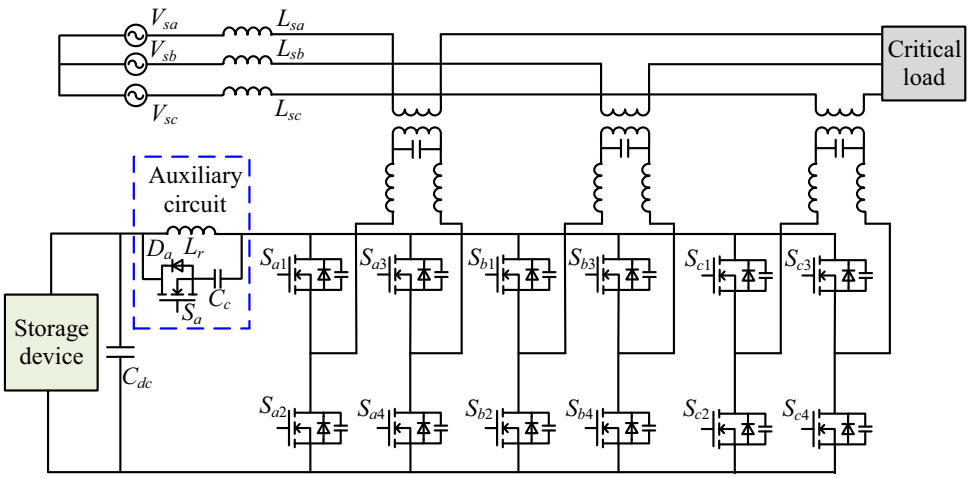

Fig. 20 ZVS converter for DVR

The unified power flow controller (UPFC) [32] or the unified power quality controller (UPQC) [33] combines the functions of the STATCOM and SSSC or DVR. It consists of two converters connected back-to-back, as shown in Fig. 21. One is connected in series with the grid, whereas the other is connected in parallel. Each converter can generate reactive power at its own AC output terminal. By inserting the auxiliary circuit into the middle DC link, both converters can realize ZVS operation. More significant efficiency improvement can be obtained as there are six bridges working in the soft-switching condition in this topology.

The ZVS AC-DC-AC topology can also be applied in the power distribution system to interconnect two AC grids with different frequencies and voltage levels, as shown in Fig. 22. For example, two micro-grids can be interconnected to enhance the security and reliability of each system. Bidirectional power flow management among the micro grids can adaptively distribute power generation according to the load condition of each system. The power loss of the AC-DC-AC interlinking converter is an important issue when the energy exchange becomes very frequent among different grids. The adoption of the ZVS technique can reduce the power loss and enhance the energy exchange efficiency.

4 Experimental verification

To verify the operation performance of the proposed ZVS technique, a 10 kVA three-phase four-wire ZVS BTB converter prototype based on the SiC MOSFET device, as shown in Fig. 23 [15], is built with the parameters listed in Table 1. The MOSFET devices used for the main switches S_{i1}-S_{i6} and S_{o1}-S_{o6} are SCT2080KE. The MOSFET device used for the auxiliary switch S_7 is C2M0025120D.

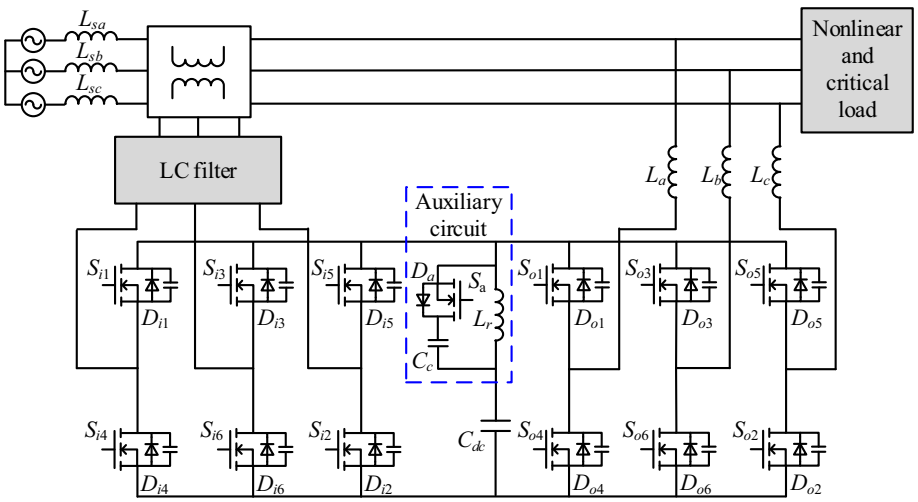

Fig. 21 ZVS converter for UPFC/UPQC

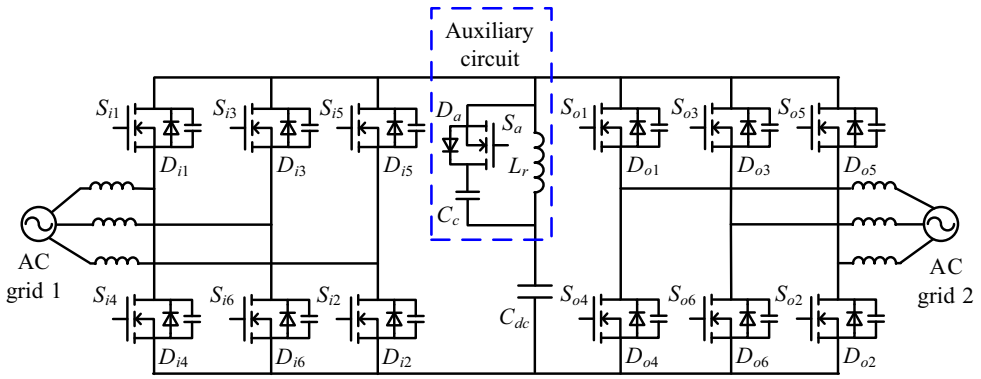

Fig. 22 ZVS AC-DC-AC converter for AC grids connection

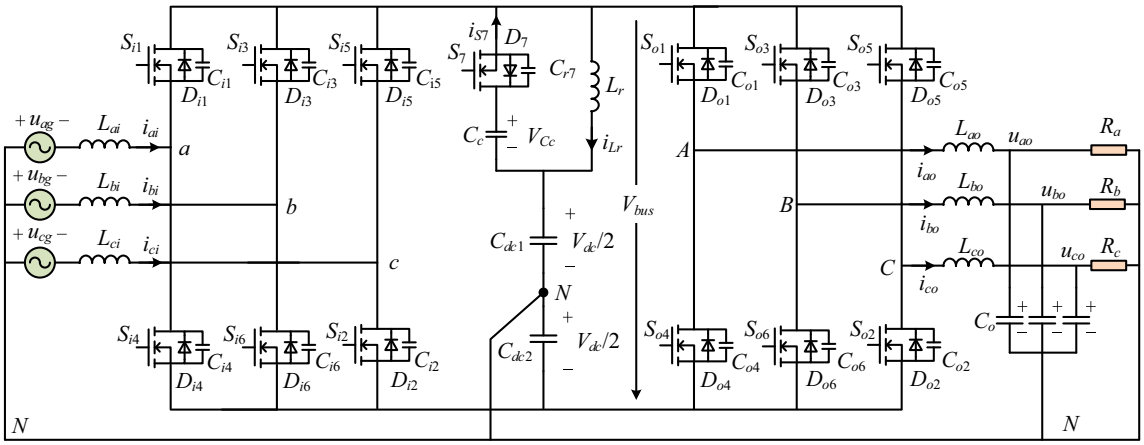

Fig. 23 ZVS BTB converter of the experimental prototype

Table 1 Parameters of prototype

Parameters	Symbol	Value
Input line voltage	U_{grms}	380 V
Output line voltage	U_{orms}	380 V
Frequency of input/output voltage	f	50 Hz
Rated power	S/P	10 kVA/9 kW
Input filter inductor	L_{ai}, L_{bi}, L_{ci}	400 μH
Output filter inductor	L_{ao}, L_{bo}, L_{co}	400 μH
Resonant inductor	L_r	2.7 μH
Resonant capacitor	C_r	0.12 nF
Clamping capacitor	C_c	66 μF
DC bus voltage	V_{dc}	700 V
Switching frequency	f_s	150 kHz

Figure A1 in Appendix A shows the picture of the ZVS BTB prototype, in which the main circuit components in the rectifier and inverter sides as well as the auxiliary circuit are demonstrated [15].

Figure 24a shows the steady state waveforms of three-phase inductor currents at the rectifier side. Figure 24b shows the three-phase output voltages at the inverter side. Both the input current and the output voltage have a low distortion waveform at the full load condition.

Figure 25 shows the waveforms of clamping capacitor voltage V_{Cc} and resonant inductor current i_{Lr} in the switching period scope. It can be seen that i_{Lr} is a triangular waveform with zero DC component in one switching period. V_{Cc} is almost constant in one switching period. DC bus voltage V_{bus} will be resonated to zero in each switching period to provide the ZVS condition.

Figures 26, 27 and 28 show the ZVS turn-on waveforms for S_{i4}, S_{o2}, and S_7, respectively, in the full load condition at different angles. The turn-on gate signals (u_{gi4}, u_{go2}, u_{g7}) are added to MOSFETs after their voltages (u_{Ci4}, u_{Co2}, u_{Cr7}) are resonated to zero in the two resonation stages. All these switches can realize ZVS turn-on after the resonation stages.

An experimental efficiency comparison is carried out at the same switching frequency of 150 kHz with the same SiC MOSFET device between the conventional hard-switching BTB converter and the ZVS BTB converter. Figure 29 shows the efficiency curves at different linear loads [15]. The ZVS BTB converter has a flatter efficiency

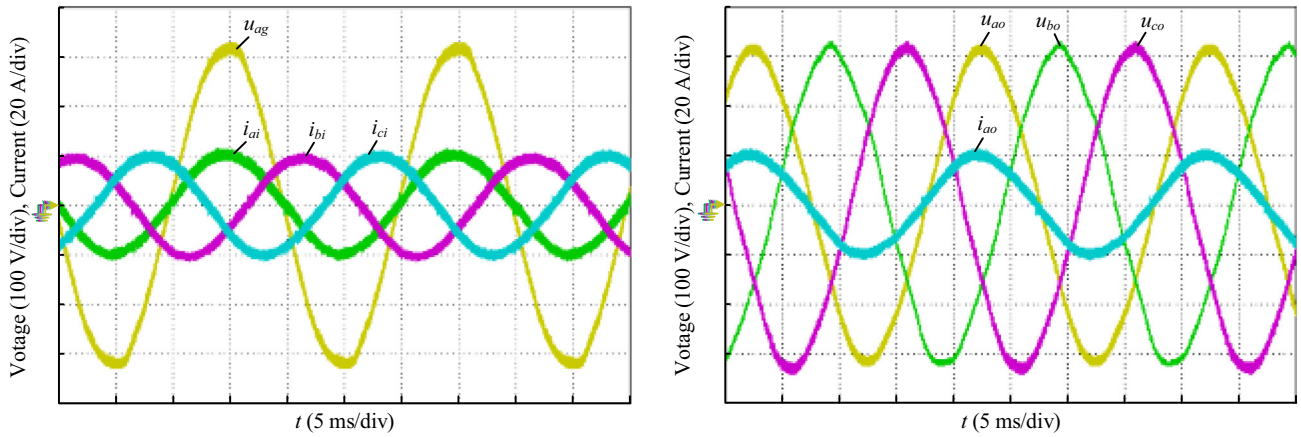

(a) Three-phase input current **(b)** Three-phase output voltage

Fig. 24 Three-phase input current and output voltage

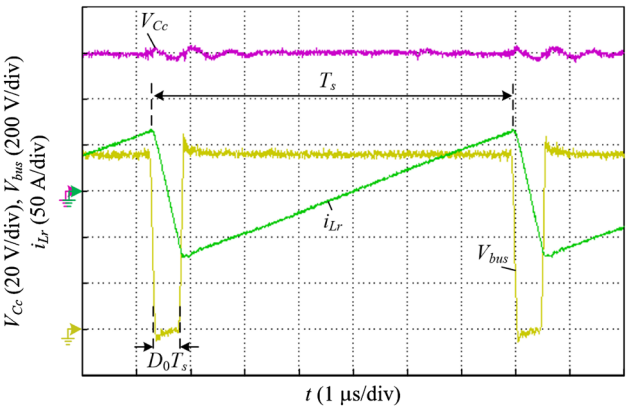

Fig. 25 Waveform of V_{Cc}, V_{bus} and i_{Lr} in one switching period

curve. It has a peak efficiency of 97.5% at half rated power. And the efficiency at rated power is over 97% as compared to 94.0% for the conventional hard-switching BTB converter. The ZVS BTB converter has an efficiency improvement of over 3% as compared with that of the conventional hard-switching BTB converter.

5 Conclusion and future work

This paper introduces a generic ZVS technique for power electronic conversion systems. With only one auxiliary circuit, all the switches of the multi-bridge converter can realize ZVS operation. Furthermore, its applications in different power electronic conversion topologies for renewable energy integration, energy storage system, and FACTS devices are discussed. Finally, a 10 kVA SiC MOSFET BTB converter prototype is built to validate the efficiency improvement of the ZVS technique compared with that in conventional hard-switching converter.

Although the ZVS converter shows promising efficiency advantage over the conventional hard-switching converter, an accurate loss model should be investigated to further optimize the system efficiency. The generic *N*-bridge ZVS circuit topology is based on the half bridge unit, which is a

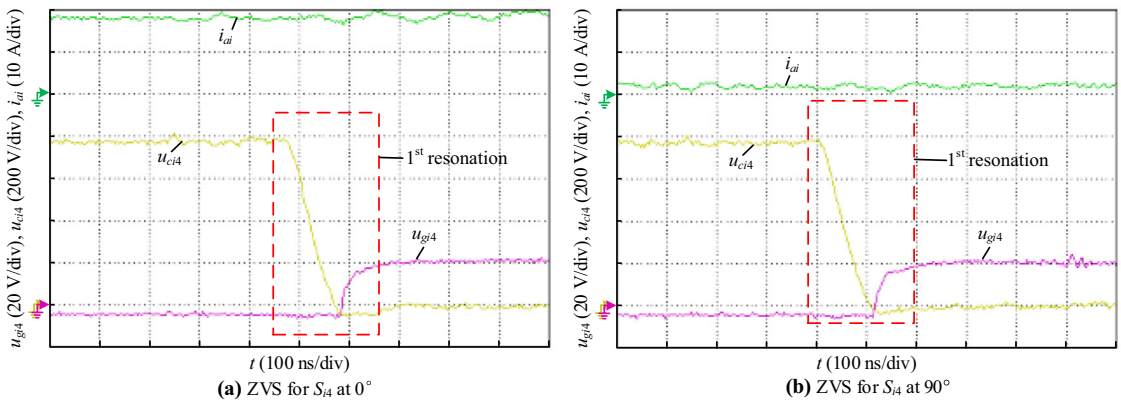

(a) ZVS for S_{i4} at 0° **(b)** ZVS for S_{i4} at 90°

Fig. 26 ZVS waveform for S_{i4}

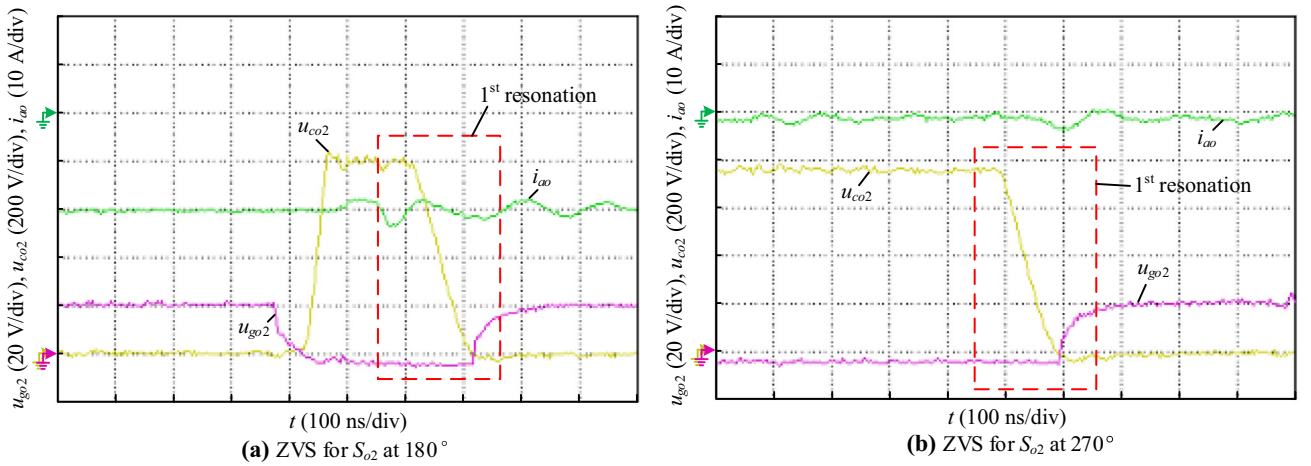

Fig. 27 ZVS waveform for S_{o2}

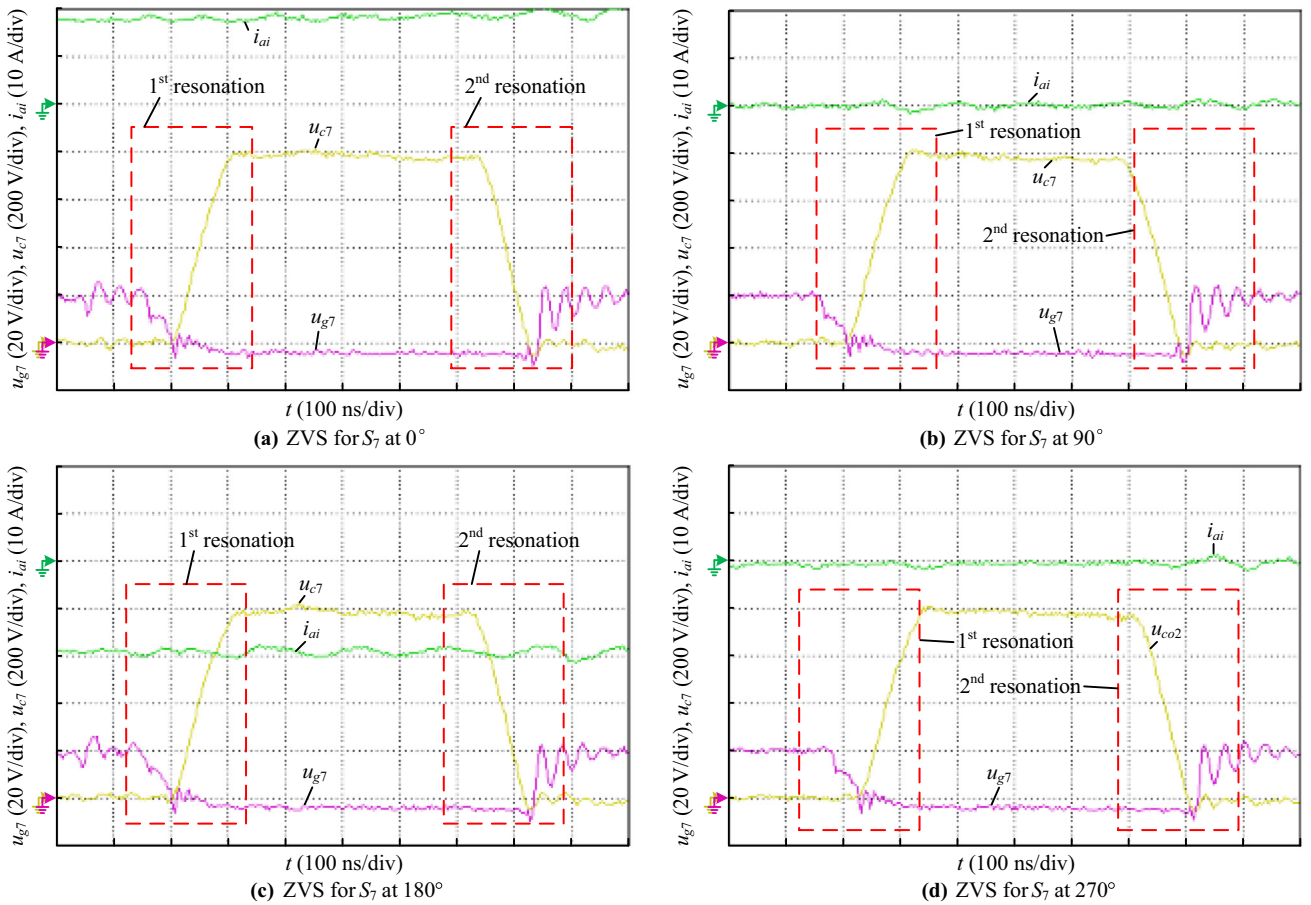

Fig. 28 ZVS waveform for S_7

two-level topology at the AC side essentially. Therefore, the reductions in volume and power loss of the AC filters are still limited as compared with those in the three-level or multilevel converter. Further studies are needed to investigate the possibility of expanding the ZVS technique to three-level or multi-level converters. The application of the ZVS technique combined with the SiC device in these converters can further improve power density and lead to a

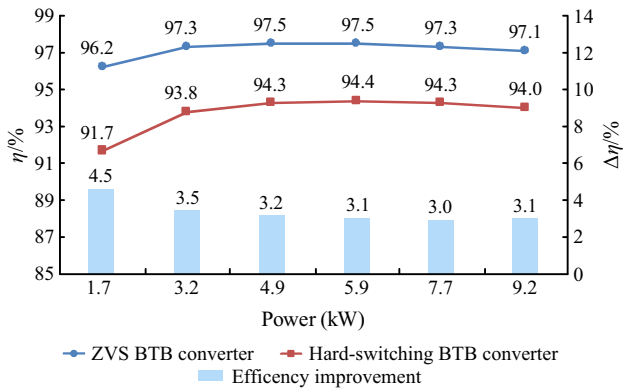

Fig. 29 Experimental efficiency curves

more compact power electronic conversion systems for high-voltage and high-power applications.

Acknowledgements This work was supported by the National Natural Science Foundation of China (No. 51777189).

Appendix A

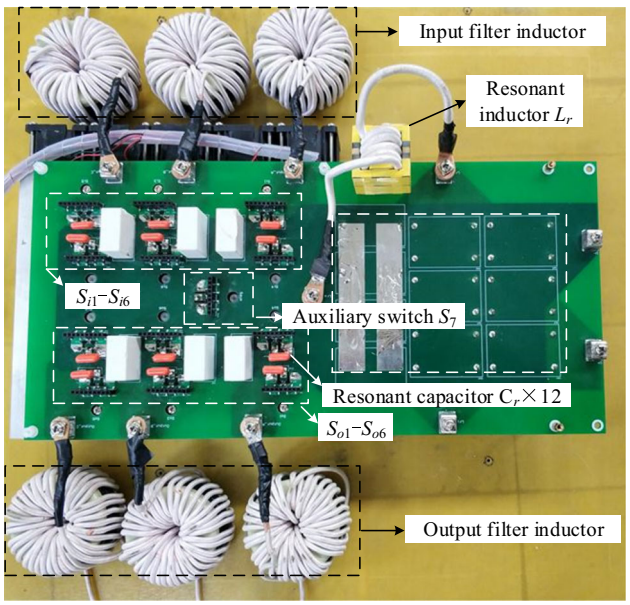

Fig. A1 Picture of prototype

References

[1] Kassakian J, Jahns T (2013) Evolving and emerging applications of power electronics in systems. IEEE J Emerg Sel Top Power Electron 1(2):47–58
[2] Millán J, Godignon P, Perpiñà X et al (2014) A survey of wide bandgap power semiconductor devices. IEEE Trans Power Electron 29(5):2155–2163
[3] She X, Huang A, Lucía Ó et al (2017) Review of silicon carbide power devices and their applications. IEEE Trans Power Electron 64(10):8193–8205
[4] Gong X, Ferreira J (2014) Investigation of conducted EMI in SiC JFET inverters using separated heat sinks. IEEE Trans Ind Electron 61(1):115–125
[5] Divan D (1989) The resonant DC link converter-a new concept in static power conversion. IEEE Trans Ind Appl 25(2):317–325
[6] Divan D, Skibinski G (1989) Zero-switching-loss inverters for high-power applications. IEEE Trans Ind Appl 25(2):634–643
[7] Yonemori H, Fukuda H, Nakaoka M (1994) Advanced three-phase ZVS-PWM active power rectifier with new resonant DC link and its digital control scheme. In: Proceedings of 5th international conference on power electronics and variable-speed drives, London, UK, 26–28 October 1994, pp 608–613
[8] Nakaoka M, Yonemori H, Yurugi K (1993) Zero-voltage soft-switched PDM three phase AC–DC active power converter operating at unity power factor and sinewave line current. In: Proceedings of power electronics specialists conference, Seattle, USA, 20–24 June 1993, pp 787–794
[9] Doncker R, Lyons J (1990) The auxiliary resonant commutated pole converter. In: Proceedings of 1990 IEEE industry applications society annual meeting, Seattle, USA, 7–12 October 1990, pp 1228–1235
[10] Yuan X, Barbi I (2000) Analysis, designing, and experimentation of a transformer-assisted PWM zero-voltage switching pole inverter. IEEE Trans Power Electron 15(1):72–82
[11] Yu W, Lai J, Park J (2010) An improved zero-voltage-switching inverter using two coupled magnetics in one resonant pole. IEEE Trans Power Electron 25(4):952–961
[12] Li R, Xu D (2014) A zero-voltage switching three-phase inverter. IEEE Trans Power Electron 29(3):1200–1210
[13] Chen Y, Xu D, Xi J et al (2016) A ZVS grid-connected full-bridge inverter with a novel ZVS SPWM scheme. IEEE Trans Power Electron 31(5):3626–3638
[14] He N, Zhu Y, Xu D (2017) Zero-voltage-switching SPWM method for three-phase four-wire inverter. In: Proceedings of IEEE applied power electronics conference, Tampa, USA, 26-30 March 2017, pp 3436-3443
[15] Shi K, Zhao A, Deng J et al (2019) Zero-voltage-switching SiC-MOSFET three-phase four-wire back-to-back converter. IEEE J Emerg Sel Top Power Electron 7(2):722–735
[16] Deng J, Shi K, Zhao A et al (2019) A universal zero-voltage-switching technique for multi-phase AC/DC converter. In: Proceedings of IEEE applied power electronics conference, Anaheim, USA, 17–21 March 2019, pp 1204–1211
[17] Kjaer S, Pedersen J, Blaabjerg F (2005) A review of single-phase grid-connected inverters for photovoltaic modules. IEEE Trans Ind Appl 41(5):1292–1306
[18] Sun Y, Liu Y, Su M et al (2016) Review of active power decoupling topologies in single-phase systems. IEEE Trans Power Electron 31(7):4778–4794
[19] He N, Chen M, Wu J et al (2019) 20 kW zero-voltage-switching SiC-MOSFET grid inverter with 300 kHz switching frequency. IEEE Trans Power Electron 34(6):5175–5190
[20] Kouro S, Leon J, Vinnikov D et al (2015) Grid-connected photovoltaic systems: an overview of recent research and

emerging PV converter technology. IEEE Ind Electron Mag 9(1):47–61
[21] Yaramasu V, Wu B, Sen P et al (2015) High-power wind energy conversion systems: state-of-the-art and emerging technologies. Proc IEEE 103(5):740–788
[22] Vazquez S, Lukic S, Galvan E et al (2010) Energy storage systems for transport and grid applications. IEEE Trans Ind Electron 57(12):3881–3895
[23] Wang G, Konstantinou G, Townsend C et al (2016) A review of power electronics for grid connection of utility-scale battery energy storage systems. IEEE Trans Sustainable Energy 7(4):1778–1790
[24] Grainger B, Reed G, Sparacino A et al (2014) Power electronics for grid-scale energy storage. Proc IEEE 102(6):1000–1013
[25] Fernão V, Romero E, Vinnikov D et al (2010) Power converter interfaces for electrochemical energy storage systems—a review. Energy Convers Manag 86:453–475
[26] Dixon J, Mora L, Rodriguez J et al (2005) Reactive power compensation technologies: state-of-the-art review. Proc IEEE 93(12):2144–2164
[27] Lascu C, Asiminoaei L, Boldea I et al (2007) High performance current controller for selective harmonic compensation in active power filters. IEEE Trans Power Electron 22(5):1826–1835
[28] Lascu C, Asiminoaei L, Boldea I et al (2009) Frequency response analysis of current controllers for selective harmonic compensation in active power filters. IEEE Trans Ind Electron 56(2):337–347
[29] Arya S, Singh B, Niwas R et al (2016) Power quality enhancement using DSTATCOM in distributed power generation system. IEEE Trans Ind Appl 52(6):5203–5212
[30] Gyugyi L, Schauder C, Sen K (1997) Static synchronous series compensator: a solid-state approach to the series compensation of transmission lines. IEEE Trans Power Deliv 12(1):406–417
[31] Nielsen J, Blaabjerg F (2005) A detailed comparison of system topologies for dynamic voltage restorers. IEEE Trans Ind Appl 41(5):1272–1280
[32] Gyugyi L (1991) A unified flow control concept for flexible AC transmission systems. In: Proceedings of international conference on AC and DC power transmission, London, UK, 17–20 September 1991, pp 19–26
[33] Khadkikar V (2012) Enhancing electric power quality using UPQC: a comprehensive overview. IEEE Trans Power Electron 27(5):2284–2297

Keyan SHI received the B.S. degree in electronic and information engineering from the College of Electrical Engineering, Zhejiang University, Hangzhou, China, in 2010. He is currently working towards the Ph.D. degree in electrical engineering. His research interests include high efficiency power conversion system and its control strategy.

Jinyi DENG received the B.S. degree in school of information science and engineering, Central South University, Changsha, China, in 2017. He is currently working towards the Ph.D. degree in electrical engineering at Zhejiang University, Hangzhou, China. His research interests include resonant converters and high efficiency power supply.

An ZHAO received the B.S. degree from Department of Electrical Engineering, Shanghai University of Engineering Science, Shanghai, China, in 2013. He is currently working towards the master degree in power electronics at Zhejiang University, Hangzhou, China. His research interests include soft-switching techniques in AC/DC converter.

Dehong XU received the B.S., M.S., and Ph.D. degrees from the Department of Electrical Engineering, Zhejiang University, Hangzhou, China, in 1983, 1986, and 1989, respectively. Since 1996, he has been with the College of Electrical Engineering, Zhejiang University, China, as a Full Professor. He was a Visiting Scholar in the University of Tokyo, Japan, from June 1995 to May 1996. From June to December 2000, he was a Visiting Professor in Center for Power Electronics Systems (CPES) of Virginia Tech, USA. From February 2006 to April 2006, he was a Visiting Professor in ETH, Switzerland. His current research interests include power electronics topology and control, power conversion for energy saving and renewable energy.